arXiv:1302.2896v1 [cond-mat.soft] 12 Feb 2013

Localization dynamics of fluids in random confinement

Thomas O. E. Skinner[1], Simon K. Schnyder[2], Dirk G. A. L. Aarts[1], Jürgen Horbach[2*], and Roel P. A. Dullens[1†]
[1]*Department of Chemistry, Physical and Theoretical Chemistry Laboratory,*
University of Oxford, South Parks Road, Oxford OX1 3QZ, United Kingdom,
[2]*Institut für Theoretische Physik II, Heinrich-Heine-Universität Düsseldorf, Universitätsstraße 1, 40225 Düsseldorf, Germany*

The dynamics of two-dimensional fluids confined within a random matrix of obstacles is investigated using both colloidal experiments and molecular dynamics simulations. By varying fluid and matrix area fractions in the experiment, we find delocalized tracer particle dynamics at small matrix area fractions and localized motion of the tracers at high matrix area fractions. In the delocalized region, the dynamics is diffusive at long times, while in the localized regime anomalous diffusion at intermediate times and trapping in finite pockets of the matrix is observed. These observations are found to agree with the simulation of an ideal gas confined in a weakly correlated matrix.

Introduction. An understanding of the dynamics in disordered heterogeneous media is of great interest for a wide range of fields like materials science, geophysics or biology [1–3]. The mass transport in such media is associated with a strong separation of time scales, i.e. there are typically mobile particles that move through a "matrix of immobile" particles. Experimental realizations of such systems are binary mixtures of colloids with disparate sizes [4, 5], other examples are ion-conducting glasses [6–10] or biological systems like cells [3].

To model such heterogeneous systems one often considers the matrix particles as being fixed in space. One of the simplest models of this type is the disordered Lorentz gas [11, 12] where a single tracer particle moves in a matrix of fixed, overlapping hard spheres that are randomly distributed in space. This model exhibits a delocalization-to-localization transition which is associated with a critical percolation point [13] of the void space accessible for the tracer particles. Whereas at low matrix densities the void space forms a percolating network leading to diffusive motion of the tracer particle, above the critical percolation density the void space becomes disconnected and the tracer particle is trapped in finite pockets of the matrix. At the critical point of the localization transition, the long-time diffusion of the tracer particle is anomalous [14–16], as reflected by a sublinear increase of the mean-squared displacement (MSD), $\delta r^2(t) \sim t^x$ with $x \approx 2/3$ in two dimensions (2D) [16] and $x \approx 0.32$ in 3D [15].

It is an open question as to whether the localization scenario of the Lorentz model is also relevant in more realistic and complex heterogenous media like ion-conductors or porous materials. Simulations have reported anomalous diffusion and localization dynamics in a range of more realistic heterogeneous systems such as binary mixtures with a frozen-in matrix component [17–22] or with a disparate size ratio of the species [23] as well as realistic models of ion-conducting alkali silicate glasses (see, e.g., [8]). The latter studies are corroborated by calculations in the framework of the mode coupling theory of the glass transition [24]. This theory provides a qualitative description of the Lorentz gas [25] and predicts localization transitions as in the Lorentz gas for disparate-sized binary mixtures [26] and quenched-annealed systems [27–30].

While models like the Lorentz gas are very instructive for the understanding of the dynamics in heterogeneous media, experimental realizations of systems with fixed, randomly-placed matrix particles are very rare. Most of the experimental studies of particle diffusion in disordered media have been reported for porous glasses [31] where systematically controlling and varying the pore size distribution and connectivity is very difficult. In this Letter, we present a 2D colloidal model experiment consisting of small tracer particles in a random confining matrix of fixed large particles, that shows delocalized tracer particle motion at low matrix area fractions and highly localized tracer dynamics at high matrix area fractions. The experimental observation of localized dynamics is supported by molecular dynamics (MD) simulations where we consider a 2D binary mixture of soft spheres with the large species being fixed and the small species forming an ideal fluid of non-interacting particles.

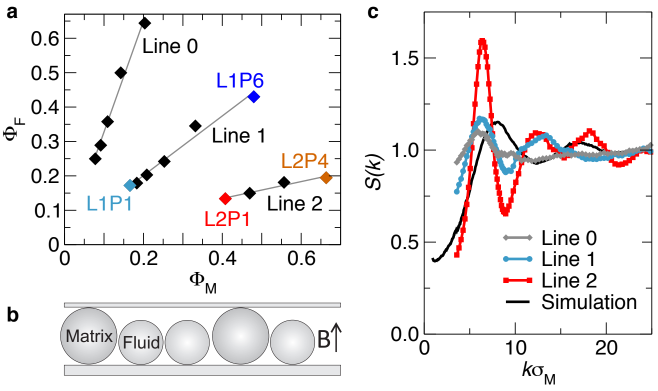

Figure 1: a) State diagram for the effective area fractions of the fluid (Φ_F) versus the matrix particles (Φ_M). b) Schematic of a two-dimensional cell with the 4.95 µm matrix particles acting as spacers. c) Structure factors for the matrix-matrix contributions for lines 0, 1 and 2 and the simulation.

Experiment. A binary colloidal mixture of 3.9 µm and 4.95 µm diameter super-paramagnetic polystyrene spheres

---

[*] e-mail: horbach@thphy.uni-duesseldorf.de
[†] e-mail: roel.dullens@chem.ox.ac.uk

(microParticles) dispersed in water is confined between two glass slides to make a two-dimensional (2D) sample cell as illustrated in Fig. 1b. The large particles act as spacers between the glass slides and hence form the fixed matrix in which the small particles – the fluid – are free to move [32]. Video microscopy is used to image an area of 430 μm × 340 μm for typically up to two hours. Standard particle tracking procedures are used to find the matrix and fluid particle coordinates [33] as a function of time from which we computed the static and dynamics quantities of interest.

We control the effective area fractions of both the matrix ($\phi_{\rm M}$) and fluid ($\phi_{\rm F}$) particles *in-situ* by applying a perpendicular external magnetic field B which leads to a repulsive pair potential given by $U_{F,M}(r) = \frac{\mu_0 \chi_{F,M}^2 B^2}{4\pi r^3}$, where r is the distance between two particles, μ_0 the permeability of free space and $\chi_{F,M}$ the magnetic susceptibility of the fluid or matrix particles. To obtain $\phi_{\rm M}$ and $\phi_{\rm F}$ we calculate the fluid and matrix particle effective hard sphere diameters $\sigma_{\rm F,M}$ using a Barker-Henderson approach according to $\sigma_{\rm F,M} = \sigma^0_{\rm F,M} + \int_{\sigma^0_{\rm F,M}}^{\infty}\left(1 - e^{-\beta U_{\rm F,M}(r)}\right) dr$, where $\sigma^0_{\rm F,M}$ are the hard sphere diameters in the absence of a magnetic field and $\beta = 1/k_B T$ [34, 35]. This approach enables us to very efficiently probe the dynamics of the fluid particles at different effective matrix and fluid area fractions *without* changing the matrix configuration. Note that the resultant effective matrix to fluid particle size ratio remains fairly constant at 0.787 as is also evident from the linear paths in the $(\phi_{\rm F}, \phi_{\rm M})$ state diagram (Fig. 1a). Our experimental state points are represented by three lines, denoted line 0, 1 and 2, in the $(\phi_{\rm M}, \phi_{\rm F})$ state diagram as shown in Fig. 1a. The lowest point in each line was obtained with no magnetic field. In our analysis, we will focus on the lowest and highest state points of line 1 and 2, which are labeled as 'L1P1' and 'L1P6' for line 1 and 'L2P1' and 'L2P4' for line 2, respectively.

To characterize the structural correlations within the matrix we computed its static structure factor $S(k) = \frac{1}{N_M}\left\langle \sum_i^{N_{\rm M}} \sum_{j\neq i}^{N_{\rm M}} {\rm e}^{-i\vec{k}\cdot(\vec{r}_i - \vec{r}_j)} \right\rangle$. Here $N_{\rm M}$ is the number of matrix particles, $\langle . \rangle$ represents an ensemble average and $\vec{r}_i$ and $\vec{r}_j$ are the positions of matrix particles i and j, respectively. The structure factors for the matrices corresponding to line 0, 1 and 2 only show weak fluid-like structural correlation (Fig. 1c), similar to the uncorrelated Lorentz model. Note that the structure factors for the matrices do *not* change along each line, which is a direct consequence of our approach to increasing the effective matrix and fluid area fractions by increasing the magnetic field. Importantly, it also directly confirms the fixed nature of the matrix particles.

We analyzed the fluid particle dynamics of all state points by computing the corresponding MSD according to $\delta r^2(t) = \frac{1}{N_{\rm F}}\left\langle \sum_{i=1}^{N_{\rm F}} [\vec{r}_i(t) - \vec{r}_i(0)]^2 \right\rangle$, with $N_{\rm F}$ the number of fluid particles and $\vec{r}_i$ the position of fluid particle i. The resulting MSDs along lines 1 and 2 are shown in Fig. 2a. Note that the shift in the short-time diffusion between the two lines is due to the different number densities [36, 37]. At L1P1, characterized by low matrix and low fluid area fractions, the tracer dynamics is diffusive at long times. Upon increasing the effective area fractions $\phi_{\rm F}$ and $\phi_{\rm M}$ along line 1, the dynamics show a noticeable slowing down and strongly sub-diffusive behavior at intermediate times. However, at long times the MSDs of all the state points along line 1 exhibit diffusive behaviour, corresponding to delocalized motion. Consistently, at all state points along line 0, i.e. at lower matrix area fractions, the tracer particles show delocalized motion as well (data not shown). Remarkably, the fluid particle dynamics exhibit completely different behavior along line 2, i.e. at much higher matrix area fractions. At L2P1, the MSD exhibits a plateau at long times, which upon increasing the effective area fractions ϕ_F and ϕ_M along line 2, decreases to smaller values. This behaviour clearly indicates the localization of the tracer particles in this region of the state diagram and shows that the length scale associated with the localization becomes smaller as the matrix area fraction is increased.

Simulation. To gain more insight into the mechanism of the experimentally observed localized tracer dynamics, we performed detailed MD simulations of a quenched-annealed system: a binary system of purely repulsive soft spheres with WCA interaction potential, where the matrix particles are fixed. In particular, we simulate the tracer dynamics in the limit of $\phi_{\rm F} \to 0$, while we systematically increase the matrix area fraction, which enables us to efficiently sample the regions corresponding to both delocalized and localized tracer dynamics.

In the MD simulations, the matrix particle diameters are sampled equidistantly, $\sigma_{\rm M} \in [0.85, 1.15]$, to avoid crystallization. The fluid particles are non-interacting to avoid the effect of fluid-fluid interaction on the dynamics. The interaction potential is $U_{\alpha\beta}(r) = 4\varepsilon_{\alpha\beta}[(\sigma_{\alpha\beta}/r)^{12} - (\sigma_{\alpha\beta}/r)^6] + \varepsilon_{\alpha\beta}$ for $r < r_{\rm cut} = 2^{1/6}\sigma_{\alpha\beta}$ and zero otherwise, with $\alpha, \beta \in ({\rm F}, {\rm M})$. The particle diameters are given by $\sigma_{\alpha\beta} = (\sigma_\alpha + \sigma_\beta)/2$, the energy scales by $\varepsilon_{\rm MM} = 1$, $\varepsilon_{\rm MF} = 0.1$, and $\varepsilon_{\rm FF} = 0$ and the masses are set to $m_{\rm M} = m_{\rm F} = 1$. Continuity of energy and forces at $r_{\rm cut}$ is ensured with the smoothened potential $U_{\alpha\beta}(r) \times (r - r_{\rm cut})^4/[h^4 + (r - r_{\rm cut})^4]$ with $h = 0.005\sigma_{\rm MM}$. The velocity-Verlet algorithm is used to integrate Newton's equations of motion with time step $\delta t = 7.2 \times 10^{-4} t_0$, where $t_0 = [m_{\rm M}\sigma_{\rm M}^2/(\varepsilon_{\rm MM})]^{1/2} = 1$.

For each realization of the system, between 1000 and 4000 matrix particles are equilibrated at number density $\rho = 0.278\sigma_{\rm M}^{-2}$ at the temperature $k_{\rm B}T = 1$ by randomly selecting the particle velocities from the Maxwell distribution every 100 steps, for 10^5 time steps. Then, the matrix particles are fixed and their positions are uniformly rescaled to $\rho = 0.625\sigma_{\rm M}^{-2}$. The computed quantities are averaged over 100 independent matrix configurations. To simulate the tracer dynamics we insert up to 1000 non-interacting fluid particles into each matrix configuration. We vary the tracer particle diameter, which is equivalent to varying the matrix area fraction *without* changing the structure of the matrix, analogous to the experiments. At each diameter the system is equilibrated for 10^6 time steps, after which we start our production runs in the microcanon-

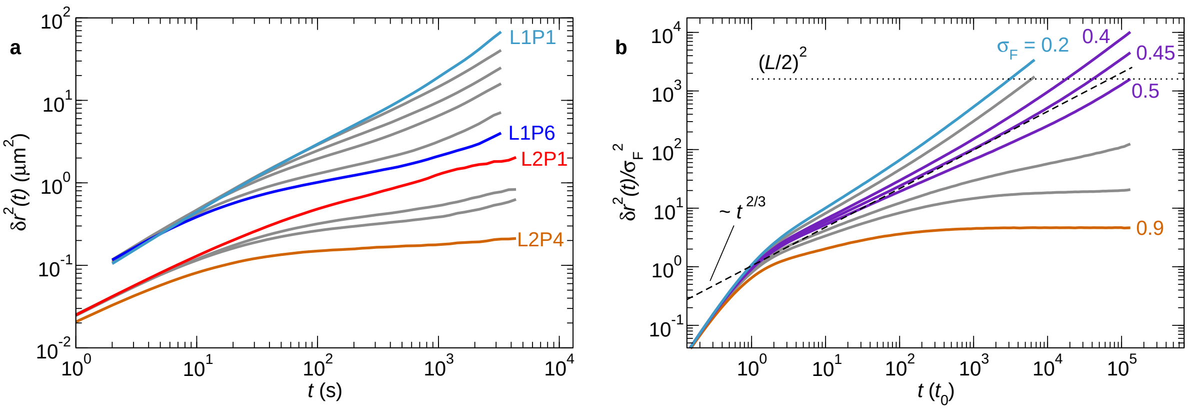

Figure 2: a) MSDs for the fluid particles in the experiment along lines 1 and 2. b) Mean square displacements for the fluid particles in the simulation for fluid particle diameters $\sigma_F = 0.2$, 0.3, 0.4, 0.45, 0.5, 0.6, 0.7, and 0.9. The dotted line roughly marks the limit above which finite size effects become important (with simulation box size L).

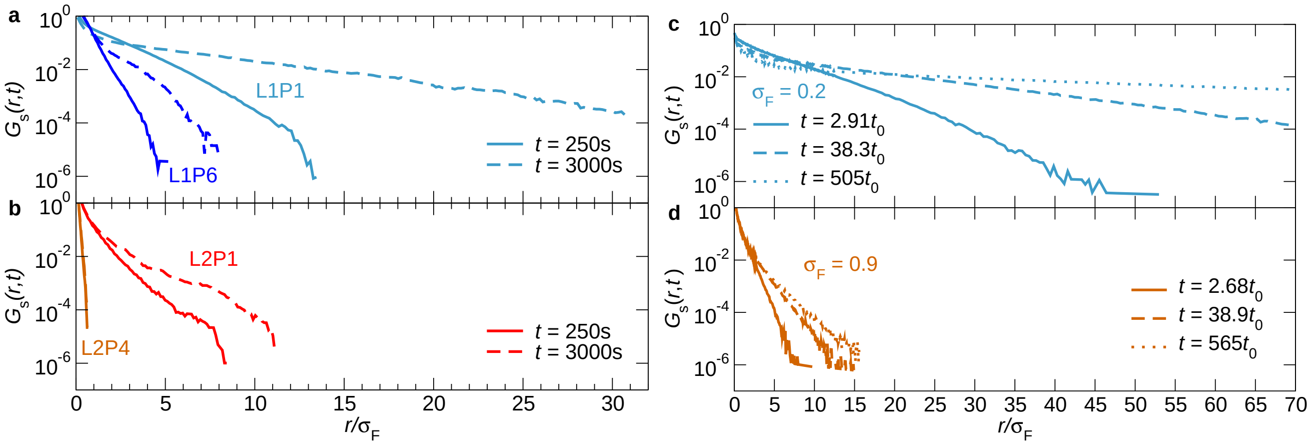

Figure 3: a) Self-part of the van Hove correlation function for the fluid particles along line 1 at state points 1 and 2 after 250s and 3000s. b) As a), but for line 2. Self-part of the van Hove correlation function for the fluid particles in the simulation for c) a delocalized state, d) an intermediate case and c) a localized state.

ical ensemble. Varying the system size L allows to control finite size effects, which only start to play a role after the MSD exceeds $\approx (L/2)^2$ as indicated in Fig. 2b.

Comparison between simulation and experiment. We computed the structure factor for the matrix particles in the simulation, which is shown in Fig. 1c). Consistent with the experiments, it shows weak fluid-like structural correlations.

In Fig. 2b we present the mean square displacements for the simulations for increasing σ_F – which is equivalent to increasing ϕ_M. In the long-time limit, the MSD changes from diffusive at small diameters – i.e. low ϕ_M – to localized at large diameters – i.e. high ϕ_M – with an extended subdiffusive regime at intermediate times. This clearly indicates that the system undergoes a transition from delocalized to localized dynamics. While at short times the motion of the tracer particles is ballistic ($\delta r^2 \propto t^2$) and thus different from the experiment, the curves qualitatively match the experimental data in Fig. 2a at intermediate and long times. The anomalous diffusion is most pronounced for $0.4 \leq \sigma_F \leq 0.5$, where we find a power law, $\delta r^2 \sim t^x$, with $x \approx 2/3$ the exponent predicted for the Lorentz model [16]. The rounding of the localization transition in our simulations is a direct consequence of the soft sphere interactions [38]. The simulated MSD curves closely match the experimental data in Fig. 2a: the experimental MSDs for line 1 closely resemble the simulated MSDs in the delocalized region ($\sigma_F \leq 0.4$), while the MSDs for line 2 are consistent with the simulated MSDs in the localized region ($\sigma_F > 0.5$).

We also computed the self-part of the van Hove correlation function [39] $G_s(r,t)$ for the experiments and the simulations as it gives the full spatial information for the tracer particle dynamics at a given time. This function gives the distribution of displacements $\Delta r_i = |\vec{r}_i(t) - \vec{r}_i(0)|$ of a tagged particle i at time t, $G_s(r,t) = \frac{1}{N_F}\left\langle \sum_{i=1}^{N_F} \delta\left(r - \Delta r_i\right)\right\rangle$. In Fig. 3a, we show the experimental van Hove correlation functions for L1P1 and L1P6 at times $t = 250$ s and $t = 3000$ s. The lower time (250 s, solid lines) roughly corresponds to the time where sub-diffusion is strongest, while the larger time (3000 s, dashed lines), marks the end of the experimental runs. The delocalized nature of the fluid particles at low area fractions is reflected by the broad distribution at L1P1 and its time dependence: the width of this distribution increases by about a factor of 3 from $t = 250\,\mathrm{s}$ to $t = 3000\,\mathrm{s}$. At point L1P6, the shape of $G_\mathrm{s}(r,t)$ is very similar compared to L1P1 but the distributions are less broad at both times. The van Hove correlation functions for L2P1 and L2P4 are presented in Fig. 3b. While L2P1 is characterized by a far lower fluid area fraction compared to L1P6, the $G_\mathrm{s}(r,t)$ of these two points are fairly similar. The localization of the system at L2P1 can only be inferred from the time-dependence, i.e. from the MSD. The $G_\mathrm{s}(r,t)$ for L2P4 indicates a strong localization as is inferred from the very narrow distribution and the absence of any shift when changing from $t = 250\,\mathrm{s}$ to $t = 3000\,\mathrm{s}$.

In the simulation, we display the van Hove function at three times to compare to the experiment, where the values of the MSD roughly agree with those of the experiment: $t \approx 3t_0$, $t \approx 39t_0$ and an additional time that is order of magnitude larger, $t \approx 550t_0$. The shape of $G_\mathrm{s}(r,t)$ of the simulation at $\sigma_\mathrm{F} = 0.2$ (Fig. 3c), matches the $G_\mathrm{s}(r,t)$ of L1P1 (Fig. 3a) well. As σ_F increases, $G_\mathrm{s}(r,t)$ in the simulation undergoes the same qualitative development as in the experiment. On the localized side at $\sigma_\mathrm{F} = 0.9$ (Fig. 3d), a very narrow distribution is observed that shows virtually no change of $G_\mathrm{s}(r,t)$ with time, except from a small broadening which qualitatively matches with our observations at L2P1 and L2P4.

The general agreement between experiment and simulation shows that fluid-fluid interactions are not important in the experiment. This is also indicated by the fact that there is no sign of particle hopping in the experimental $G_\mathrm{s}(r,t)$ which would be reflected in peaks or shoulders around the nearest-neighbor distance between tracer particles (note that also the quantity $2\pi r G_\mathrm{s}(r,t)$ does not show such a feature) [8, 18, 38].

Conclusion. A combination of an experimental colloidal model system and MD simulation has been used to study the dynamics of two-dimensional fluids confined in a random matrix of obstacles. In the experiments, mean squared displacements and van Hove correlation functions show signatures of delocalized tracer dynamics at low matrix area fractions and localized motion at high matrix area fraction. In particular, we observe long-time diffusion at small matrix area fractions, while anomalous diffusion at intermediate times and trapping in finite pockets of the matrix is present at high matrix area fractions. The simulation of an ideal gas confined in a weakly correlated matrix shows qualitative agreement with the experiment. Around the percolation point of the localization transition, the mean squared displacements, as obtained from the simulation, exhibit power-law-like anomalous diffusion over multiple time decades compatible with the predicted exponent of the two-dimensional Lorentz model.

Our experimental model system provides an ideal system for the investigation of transport in strongly heterogeneous media. The interactions between the tracer particles are tunable, the number density of the tracer particles can be varied and it is possible to introduce external fields by using optical tweezers or, in the case of charged tracer particles, an electric field. Thus, it is possible to study the change of transport properties from Lorentz gas-like localization scenario to the "usual" glass transition in porous confinement if one increases the density of tracer particles, and, in doing so, one can probe the nonlinear response to external fields.

We thank Pinaki Chaudhuri for useful discussions. SKS and JH acknowledge the DFG research unit FOR-1394 "Nonlinear response to probe vitrification" (project P8) for financial support. TOES, DGALA and RPAD acknowledge EPSRC for financial support.

[1] M. Sahimi, Rev. Mod. Phys. **65**, 1393 (1993).
[2] D. B. Dingwell, Science **273**, 1054 (1996).
[3] F. Höfling and T. Franosch, to appear in Rep. Prog. Phys. (2013).
[4] A. Imhof and J. K. G. Dhont, Phys. Rev. E **52**, 6344 (1995).
[5] A. Imhof and J. K. G. Dhont, Phys. Rev. Lett. **75**, 1662 (1995).
[6] A. K. Jonscher, Nature **267**, 673 (1977).
[7] A. Bunde, K. Funke, and M. D. Ingram, Solid State Ionics **105**, 1 (1998).
[8] J. Horbach, W. Kob, and K. Binder, Phys. Rev. Lett. **88**, 125502 (2002).
[9] T. Voigtmann and J. Horbach, EPL **74**, 459 (2006).
[10] J. C. Dyre, P. Maass, B. Roling, and D. L. Sidebottom, Rep. Prog. Phys. **72**, 046501 (2009).
[11] H. A. Lorentz, Proc. Roy. Acad. Amst. **7**, 438 (1905).
[12] H. van Beijeren, Rev. Mod. Phys. **54**, 195 (1982).
[13] D. Stauffer and A. Aharony, *Introduction to Percolation Theory* (Taylor & Francis, London, 1991).
[14] D. Ben-Avraham and S. Havlin, *Diffusion and Reactions in Fractals and Disordered Systems* (Cambridge University Press, Cambridge, 2000).
[15] F. Höfling, T. Franosch, and E. Frey, Phys. Rev. Lett. **96**, 165901 (2006).
[16] T. Bauer, F. Höfling, T. Munk, E. Frey, and T. Franosch, EPJ-ST **189**, 103 (2010).
[17] J. Kurzidim, D. Coslovich, and G. Kahl, Phys. Rev. Lett. **103**, 138303 (2009).
[18] J. Kurzidim, D. Coslovich, and G. Kahl, Phys. Rev. E **82**, 1 (2010).
[19] J. Kurzidim, D. Coslovich, and G. Kahl, J. Phys.: Condensed Matt. **23**, 234122 (2011).
[20] K. Kim, K. Miyazaki, and S. Saito, EPL **88**, 36002 (2009).
[21] K. Kim, K. Miyazaki, and S. Saito, Eur. Phys. J.-Spec. Top. **189**, 135 (2010).
[22] K. Kim, K. Miyazaki, and S. Saito, J. Phys.: Condensed Matt. **23**, 234123 (2011).
[23] T. Voigtmann and J. Horbach, Phys. Rev. Lett. **103**, 205901 (2009).
[24] W. Götze, *Complex Dynamics in Glass-Forming Liquids* (Oxford University Press, Oxford, 2009).
[25] M. Spanner, S. K. Schnyder, F. Höfling, T. Voigtmann, and T. Franosch, Soft Matter **9**, 1604 (2013).
[26] T. Voigtmann, EPL **96**, 36006 (2011).
[27] V. Krakoviack, Phys. Rev. Lett. **94**, 65703 (2005).
[28] V. Krakoviack, Phys. Rev. E **75** (2007).
[29] V. Krakoviack, Phys. Rev. E **79**, 1 (2009), arXiv:0901.3649v1.
[30] V. Krakoviack, Phys. Rev. E **84** (2011).

[31] M. C. Bellissent-funel, J. Lal, and L. Bosio, J. Chem. Phys. **98**, 4246 (1993).

[32] G. Cruz de León, J. Saucedo-Solorio, and J. Arauz-Lara, Phys. Rev. Lett. **81**, 1122 (1998).

[33] J. C. Crocker and D. G. Grier, J. Colloid Interface Sci. **179**, 298 (1996).

[34] J. A. Barker and D. Henderson, J. Chem. Phys. **47**, 4714 (1967).

[35] J. P. Hansen and I. R. McDonald, *Theory of simple liquids* (Academic Press, London, 2006).

[36] X. Qiu, X. L. Wu, J. Z. Xue, D. J. Pine, D. A. Weitz, and P. M. Chaikin, Phys. Rev. Lett. **65**, 516 (1990).

[37] Y. Peng, W. Chen, T. M. Fischer, D. A. Weitz, and P. Tong, J. Fluid Mech. **618**, 243 (2008).

[38] S. Schnyder, T. Voigtmann, and J. Horbach, unpublished (????).

[39] K. Binder and W. Kob, *Glassy Materials and Disordered Solids* (World Scientific, Singapore, 2011).